communications biology

A Nature Portfolio journal

Article

https://doi.org/10.1038/s42003-025-08134-4

Cortical representational geometry of diverse tasks reveals subject-specific and subject-invariant cognitive structures

Tomoya Nakai [1,2,3] ✉, Rieko Kubo[3,4] & Shinji Nishimoto [3,4,5]

The variability in brain function forms the basis for our uniqueness. Prior studies indicate smaller individual differences and larger inter-subject correlation (ISC) in sensorimotor areas than in the association cortex. These studies, deriving information from brain activity, leave individual differences in cognitive structures based on task similarity relations unexplored. This study quantitatively evaluates these differences by integrating ISC, representational similarity analysis, and vertex-wise encoding models using functional magnetic resonance imaging across 25 cognitive tasks. ISC based on cognitive structures enables subject identification with 100% accuracy using at least 14 tasks. ISC is larger in the fronto-parietal association and higher-order visual cortices, suggesting subject-invariant cognitive structures in these regions. Principal component analysis reveals different cognitive structure configurations within these regions. This study provides evidence of individual variability and similarity in abstract cognitive structures.

What brain properties shape our uniqueness and commonality? Cognitive neuroscience researchers have often viewed inter-individual differences as random noise. However, an increasing number of studies have quantitatively examined such variability in brain structures and functions[1–3]. These studies reported distinct subject-specific activity patterns even after anatomically aligning individuals' data into a template brain[1,4], which are highly stable across different experimental sessions[5–7]. Quantitative comparison of functional connectivity consistently found greater individual differences in the fronto-parietal association cortex, while smaller differences were observed in the early sensorimotor cortex[8–11]. Similar cortical organization of individual variability was observed in different developmental stages[12,13], suggesting a possible link with the functional hierarchy along the sensorimotor-association cortical axis[14,15].

Simultaneously, other studies assessed similarities in brain activity among individuals. A common methodology in these studies is inter-subject correlation (ISC) analysis, which calculates how temporal activity profiles or functional connectivity of different subjects synchronize when they are watching movies[16–18], listening to speech and music[19–21], speech production[22], and combining of multimodal stimuli[23]. These studies have demonstrated that ISC is larger in the low-level sensory areas and smaller in the association cortices[24,25]. As smaller individual differences in brain activity equate to similar brain activity patterns across individuals, this is likely an investigation of a similar phenomenon from a different angle.

While these approaches derive information directly from brain activity, it remains unclear how individuals differ in similarity relations among diverse cognitive tasks, which we call *cognitive structure*. For instance, while some individuals may have similar brain representations for language and visual tasks, others may have similar representations for language and auditory tasks (Fig. 1a). To examine such similarity relations, researchers developed the representational similarity analysis (RSA)[26]. This technique models representations of discrete tasks or stimuli through multivoxel activity patterns, enabling computation of cognitive structures among diverse tasks[27,28]. So far, RSA has mainly been used to investigate shared activity patterns at the group level[29–31] and to compare with behavioral patterns[32–35], but little is known about RSA's effectiveness as a basis for inter-subject variability and similarity in cognitive structures or about the brain regions that represent such variability.

We address these challenges by integrating ISC and RSA across various cognitive tasks using vertex-wise encoding models[36]. Encoding models quantitatively predict brain activity based on a combination of features from presented stimuli. This approach has been applied to model brain response patterns in visual[37–39], auditory[40,41], emotion[42,43], language[44–46], and mathematical domains[47,48]. The weight matrices obtained during the encoding model construction reflect how target features are represented in the brain[27,43], facilitating subsequent RSA and ISC analyses based on the model weights.

[1]Araya Inc, Tokyo, Japan. [2]Lyon Neuroscience Research Center (CRNL), INSERM U1028 - CNRS UMR5292, University of Lyon, Bron, France. [3]Center for Information and Neural Networks, National Institute of Information and Communications Technology, Suita, Japan. [4]Graduate School of Frontier Biosciences, The University of Osaka, Suita, Japan. [5]Graduate School of Medicine, The University of Osaka, Suita, Japan. ✉e-mail: nakai.tomoya@neuro.mimoza.jp

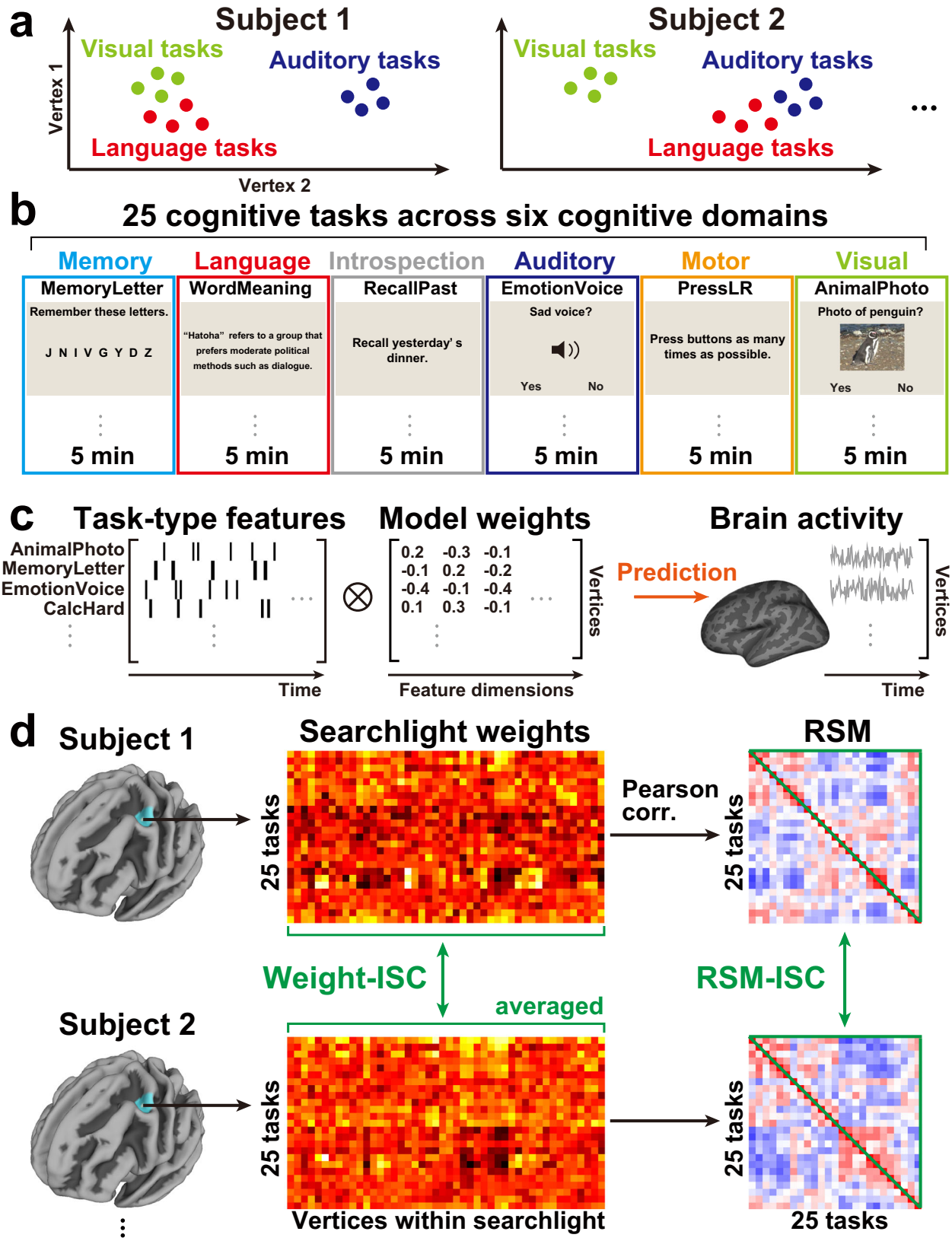

To comprehensively assess individuals' cognitive structures across a broad range of abilities, we acquired functional magnetic resonance imaging (fMRI) data from 59 subjects performing 25 tasks spanning six cognitive domains (memory, language, introspection, auditory, motor, and visual) (Fig. 1b; detailed task descriptions in Supplementary Note 5). These tasks were based on our prior studies with over 100 cognitive tasks, revealing a hierarchical organization within the six cognitive domains[27,28]. The current experimental design, a condensed version of these studies, aims to cover brain activity in most cortical areas within a 30 min timeframe per person. For each subject, we developed a vertex-wise encoding model utilizing

Fig. 1 | Evaluation of cognitive structures based on diverse tasks. a Schematic image of individual variability in cognitive structures. Tasks from three cognitive domains (visual, auditory, and language) are mapped onto the cortical representational space. **b** Subjects engaged in 25 cognitive tasks spanning six cognitive domains, with fMRI data collected during a 5 min duration for each cognitive domain. The original Japanese stimuli were translated into English for the purpose of intelligibility. **c** Vertex-wise encoding models were constructed by representing brain activity through discrete task-type features, composed of a series of one-hot vectors. Weight matrices were computed using Ridge regression. **d** In the vicinity of each target cortical vertex, weight vectors were extracted from all vertices within a 9 mm geodesic distance (searchlight) on the cortical surface. The weight-based inter-subject correlation (weight-ISC) was determined by directly comparing the weight vectors of all subject pairs, averaged within the searchlight vertices. A representational similarity matrix (RSM) was generated for each searchlight by combining the weight vectors, and the RSM-ISC was computed by comparing the upper triangular components of RSMs for all subject pairs.

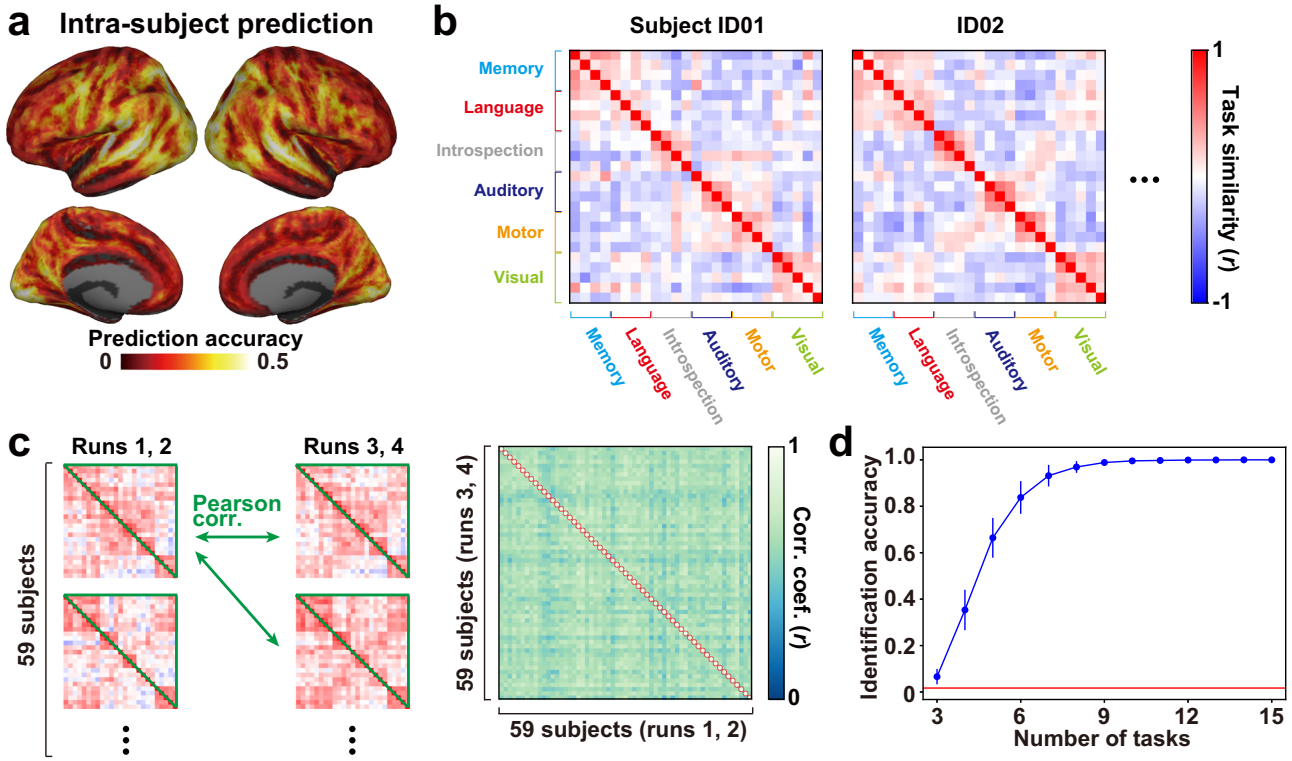

Fig. 2 | Encoding models capture subject-specific information. a The average prediction accuracy of the task-type encoding model is depicted on the standard cortical surface. The trained models are tested on the same subject (intra-subject prediction). **b** Example RSMs of two subjects calculated using all cortical vertices. Task pairs with a similar weight pattern are colored in red, while those with distinct weight patterns are in blue. **c** (Left) Schematic representation of subject identification analysis. Two half-model RSMs are obtained using data from the 1st and 2nd runs for one half, and from the 3rd and 4th runs for the second half for each subject. Their upper triangular components are compared using Pearson's correlation (Right). The correlation coefficients of the half-model RSMs are shown for all subject pairs. For each row, the identified subject is marked with a red circle. **d** The modulation of identification accuracy is plotted as a function of the varying number of tasks. The red line indicates the chance-level accuracy (1/59). Error bar, SD.

categorical task-type features and derived weight values corresponding to the 25 tasks (Fig. 1c). Subsequently, we computed ISC using searchlight-based representational similarity matrices (RSMs) among the 25 tasks (Fig. 1d). To assess the methodology's potential, we initially examined whether the encoding models and resultant RSMs effectively captured individual differences in cognitive structures. We then explored the brain organization of ISC concerning cognitive structures, visualizing these structures. Finally, we investigated how the brain organization of cognitive structures was influenced by different feature types using artificial neural network (ANN) models. This study presents evidence on the brain organization underlying individual variability and similarity in abstract cognitive structures.

Results

Encoding models capture individual variability in cognitive structures

Our initial inquiry revolves around the effectiveness of vertex-wise encoding models in capturing diverse cognitive structures among individuals. To address this, we trained a task-type encoding model for each subject using four out of the five runs and subsequently predicted brain activity in the left-out run. The intra-subject prediction performance was first assessed using the Pearson's correlation coefficient between predicted and actual signals. We observed that intra-subject encoding models robustly predicted activity across the entire cortex (prediction accuracy, mean ± SD, 0.153 ± 0.025; sign permutation test across subjects, 97.2% of vertices were significant; sign permutation test, corrected $p < 0.05$) (Fig. 2a). Similar prediction patterns were found using a block permutation test (97.4% of vertices were significant; Supplementary Fig. 1, Supplementary Note 3). Although these results do not indicate that the 25 tasks fully explain the activity patterns of the human cortex, they suggest that these tasks involve activity patterns of most cortical regions. To exclude brain regions not related to any tasks at all, we used the significant vertices in Fig. 2a as an inclusion mask for subsequent analyses.

We proceeded to assess the specificity of encoding models for individuals by applying these models to other individuals' brain activity through cross-subject prediction. For each target subject, we averaged the prediction accuracy obtained using encoding models from the other 58 subjects. Once again, we observed significant prediction across the cortex (prediction accuracy, 0.054 ± 0.007; 94.6% of vertices were significant; sign permutation test, corrected $p < 0.05$) (Supplementary Fig. 2a). Intra- and cross-subject

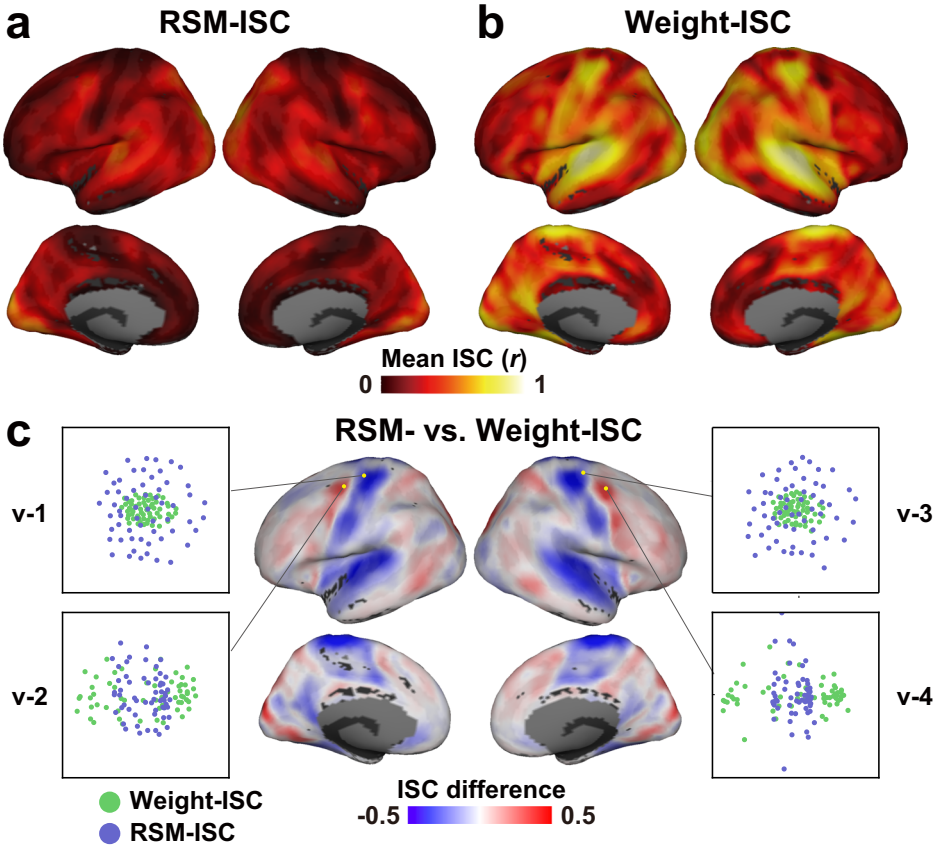

Fig. 3 | Larger RSM-ISC in higher-order brain regions. a Cortical surface mapping of Mean RSM-ISC and **b** Weight-ISC across all subject pairs. **c** Contrast between RSM-ISC and weight-ISC, where weight-ISC is corrected using the fitting curve obtained from simulation analysis and subtracted from RSM-ISC (Supplementary Fig. 5). Vertices with higher RSM-ISC are colored in red, while those with higher (corrected) weight-ISC are in blue. Scatter plots depict multidimensional scaling analysis (MDS with IDIOSCAL scaling; see Methods for details) of weight-ISC and RSM-ISC values for data from four representative vertices across the 59 subjects.

prediction accuracies displayed a high correlation (Pearson's correlation coefficient, $r = 0.828$). However, intra-subject prediction outperformed cross-subject prediction in 99.4% of cortical vertices (Supplementary Fig. 2b). These results indicate that, although task-type encoding models can exhibit some degree of generalization to other individuals, they are highly specific to each individual.

To gauge individual differences in cognitive structures, we calculated an RSM among 25 tasks for each subject using weight matrices of all cortical vertices. RSMs were constructed based on Pearson's correlation coefficients between all pairs of the 25 tasks. These RSMs demonstrated significant individual variability. For example, one subject (ID02) exhibited a substantial similarity (colored in red) between the visual and memory task domains, while another subject (ID01) displayed a lesser similarity (colored in blue) between these domains (Fig. 2b). The individual variability of task similarity (similarity variance) was relatively large in the motor task domain, and smaller in the auditory and visual task domains (Supplementary Fig. 3). For other cognitive domains, the similarity variance depended on the paired cognitive domains. Note that this variability does not indicate variance of signal-to-noise ratio (SNR) across tasks; but rather demonstrates that similarity structures across tasks are subject-specific. These findings unequivocally demonstrate the existence of distinct cognitive structures among individuals.

We proceeded to assess whether these RSMs contained sufficient information for subject identification. For this purpose, we divided the original training data into two parts (runs 1–2 and runs 3–4) and reconstructed an encoding model for each part (Fig. 2c). RSMs were then calculated based on these half-models and compared across subjects. This analysis accurately identified all subjects (identification accuracy = 1.0; mean correlation coefficient, $r = 0.928 \pm 0.020$ for the same subjects' RSMs; 0.636 ± 0.035 for the different subjects' RSMs).

Subject identification may be influenced by the task designs adopted in the experiment and the number of tasks included. To address this concern, we randomly selected a subset of the 25 tasks (ranging from three to 24 tasks) and calculated identification accuracy. The identification accuracy increased proportionally with the number of tasks included in the analysis, reaching a plateau (i.e., identification accuracy = 1.0) at 14 tasks (Fig. 2d; also see Supplementary Note 1 and Supplementary Table 1). This outcome suggests that our task set covers a much larger cognitive space than the minimal number of tasks required to identify subject-specific information.

Subject-invariant cognitive structures are represented in higher-order brain regions

We endeavored to pinpoint the brain regions reflecting subject-invariant and subject-specific cognitive structures. In pursuit of this inquiry, we derived a weight matrix from the surface searchlight around each target vertex (within a 9 mm geodesic distance) and conducted ISC analysis based on the RSMs across 25 tasks (RSM-ISC, as depicted in Fig. 1d right). Our observations unveiled relatively small RSM-ISC values around the central sulcus (CS) and superior temporal cortex, contrasting with large values in the fronto-parietal association cortices (Fig. 3a). While we utilized Pearson's correlation coefficient as a similarity index in the preceding RSM calculation, aligning with ISC literature[49], it's noteworthy that other studies have employed Spearman's correlation for comparing different RSMs[34,50]. To fortify our findings, we performed the same analysis using Spearman's correlation, yielding similar results (Supplementary Fig. 4), underscoring the resilience of our conclusions across distinct similarity indices.

The cognitive structures unveiled by the RSM-ISC encapsulate second-order information about the task weight matrix based on similarity relations. However, we did not assess whether the original weight matrices possessed the capacity to capture such cognitive structures. In pursuit of this, we calculated ISC by directly comparing model weights among subjects (weight-ISC, as depicted in Fig. 1d center). In contrast to the RSM-ISC, we identified relatively large weight-ISC values around the CS, as well as the superior temporal and occipital cortices (Fig. 3b). This dichotomy suggests that RSM-ISC and weight-ISC capture distinct facets of the brain's representations of cognitive tasks.

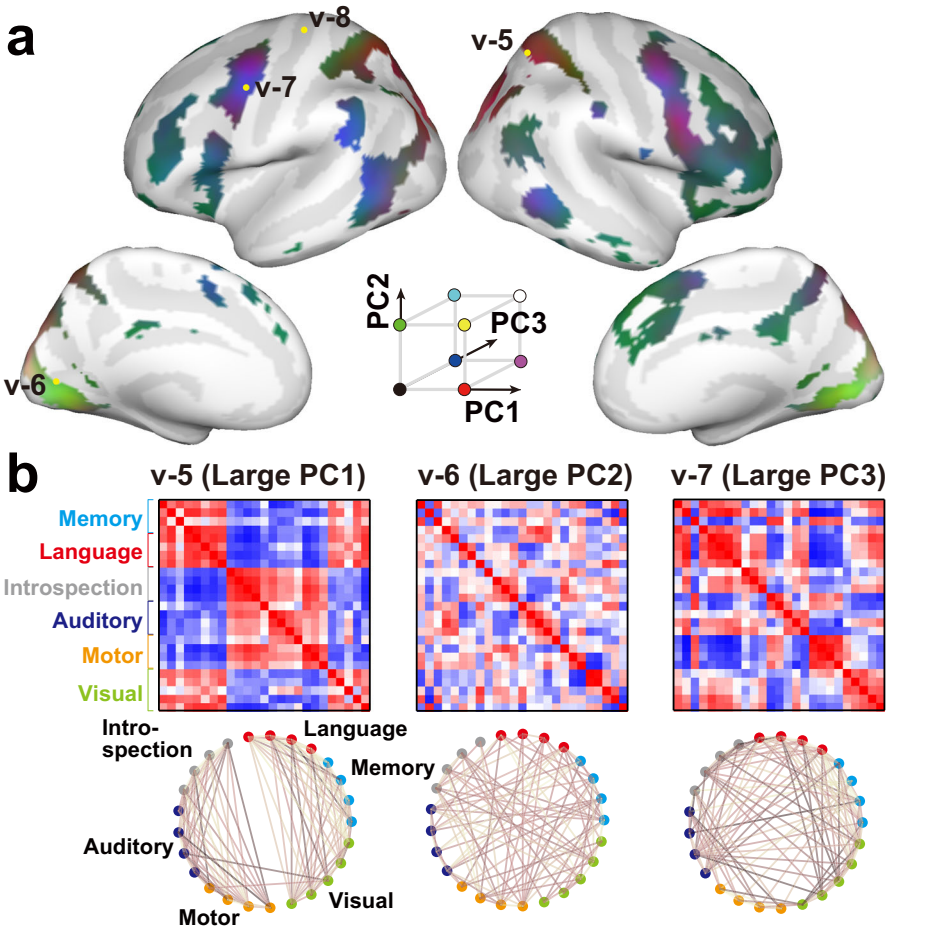

Fig. 4 | Cortical organization of subject-invariant cognitive structures. a A cortical map of distinct RSM patterns is revealed through principal component analysis (PCA). Mask vertices with a significant RSM- vs. weight-ISC value were derived from half of the subjects, and PCA was applied to the remaining subjects within the mask. Contributions of the top three PCs (PC1–PC3) are shown in red, green, and blue, respectively. **b** RSMs of three exemplary vertices (v-5, v-6, v-7) selected from (**a**), along with their network visualization. RSMs are averaged across subjects. For clarity, only task pairs with a correlation coefficient (r) > 0.2 are connected.

Directly comparing weight-ISC and RSM-ISC might be inappropriate due to the possibility that some RSM-ISC components could arise from the arrangement of weight-ISC. Specifically, a scenario could exist where RSM-ISC has a large value if there is an array of synchronized vertices with large weight-ISCs spatially arranged around the target vertex (Supplementary Fig. 5a). Computational simulations indicated that RSM-ISC values tend to increase when weight-ISC values are elevated (Supplementary Fig. 5b).

In consideration of this potential confounding factor, we corrected the weight-ISC value based on the fitting curve obtained from the simulation analysis and compared it with RSM-ISC (Fig. 3c). Our findings revealed that RSM-ISC was larger than the corrected weight-ISC in fronto-parietal association cortices, whereas the corrected weight-ISC was larger than RSM-ISC around the CS and superior temporal cortex. Analyzing the distribution of differences between RSM-ISC and weight-ISC using selected anatomical regions-of-interest (Supplementary Fig. 6, 7)[51], we observed that higher-order brain areas, including the bilateral superior occipital gyrus (SOG), middle temporal gyrus (MTG), precentral sulcus (PreCS), and superior parietal lobule (SPL), exhibited a larger RSM-ISC (difference between RSM- and weight-ISC, mean ± SD, 0.080 ± 0.042; standard deviation calculated across all subject pairs). In contrast, primary sensorimotor areas, such as the bilateral occipital pole (OP), Heschl's gyrus (HG), and CS, demonstrated a larger weight-ISC (difference between RSM- and weight-ISC, −0.222 ± 0.037). Multi-dimensional scaling (MDS) analysis further visualized how RSMs and weight matrices differed across subjects (Fig. 3c). In the vertices (blue) where weight-ISC was larger than RSM-ISC (v-1, v-3), subjects were more closely located, indicating similarity in their representations using the weight-ISC value. Conversely, in the vertices (red) where RSM-ISC was larger than weight-ISC (v-2, v-4), subjects were more closely located using the RSM-ISC value. In summary, these findings indicate that, contrary to the previous literature on activity-based ISC, subject-invariant cognitive structures are organized in fronto-parietal and higher-order visual cortices.

Distinct cognitive structures are represented on the cortical surface

The preceding analyses demonstrated the presence of subject-invariant cognitive structures in the fronto-parietal and higher-order visual areas. However, it remained uncertain whether such structures differed within these areas. To investigate this possibility, we conducted a principal component analysis (PCA) based on the vectorized upper triangular part of the RSMs, using vertices exhibiting a significantly larger RSM-ISC than weight-ISC (also see Supplementary Fig. 8 and Supplementary Note 4 for PCA using the original weight matrices). For data independence, we initially obtained a cortical mask of the RSM-vs. weight-ISC contrast (with significant vertices; sign permutation, corrected $p < 0.05$) using half of the subjects (29 subjects; ID01-ID29) and performed PCA with the remaining 30 subjects (ID30-ID59). We visualized distinct organization of cognitive structures across these areas in red, blue, and green colors corresponding to the top three principal components (PCs) (Fig. 4a, Supplementary Fig. 9; also see results with the other half of subjects in Supplementary Fig. 10). These three PCs explained 54.2% of the variances in the original RSMs (Supplementary Fig. 9).

Example vertices from each of the red, blue, and green regions clearly exhibited distinct cognitive structures. In a vertex from the red region (v-5, with a large PC1), tasks were organized separately based on their cognitive domains. Language, memory, and visual tasks constituted one cluster, while introspection, auditory, and motor tasks formed another distinct cluster

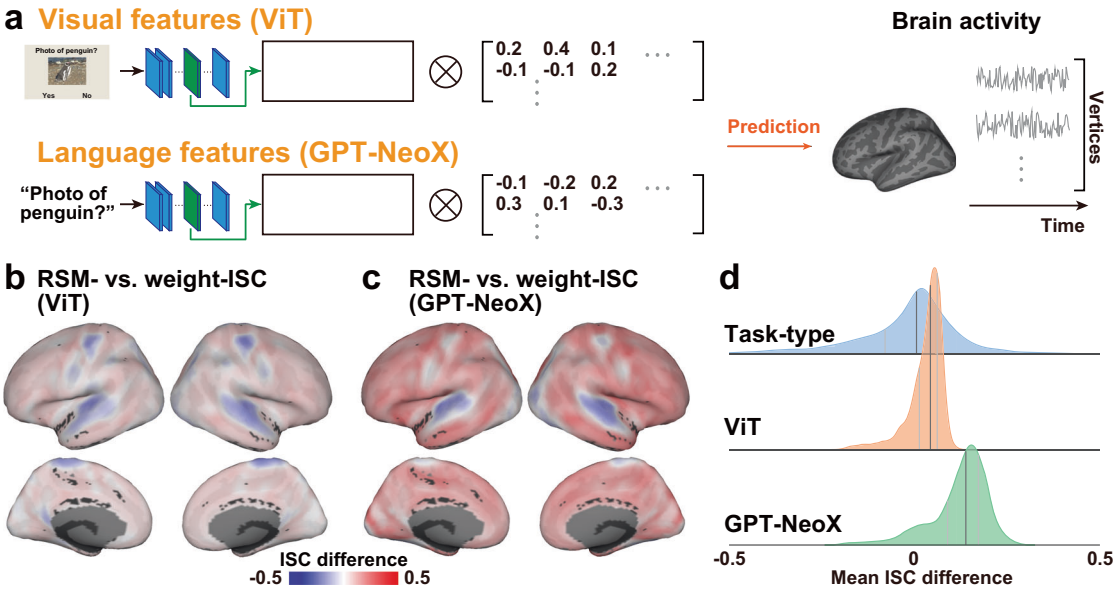

Fig. 5 | Latent neural network features exhibit similar but narrower distributions. **a** Illustration of encoding models utilizing visual (ViT) and language (GPT-NeoX) neural network features. Contrasts between RSM-ISC and weight-ISC for (**b**) visual features (ViT) and **c** language neural network features (GPT-NeoX). **d** Distributions of the difference between RSM-ISC and weight-ISC across the cortex for the three types of features (task-type, ViT, and GPT-NeoX).

(average RSM across subjects; Fig. 4b, left). In a vertex from the green region (v-6, with a large PC2), tasks were more tightly connected to tasks of different domains and did not form recognizable clusters (Fig. 4b, center). A vertex from the blue region (v-7, with a large PC3) showed an intermediate organization between the red and green vertices (Fig. 4b, right). Auditory and introspection tasks were connected to language, memory, and visual tasks, but motor tasks were not fully connected with these domains. In terms of individual RSMs, subjects displayed similar structures in the vertex with a large RSM-ISC (v-5, mean RSM-ISC = 0.45; Supplementary Fig. 11a), while no clear structure was found in the vertex with a small RSM-ISC (v-8, RSM-ISC = 0.08; Supplementary Fig. 11b).

Similar but narrower distributions are obtained using other latent features

The categorical model used in the preceding sections assumes distinct representations for different tasks, modeled by one-hot vectors. While this model-based approach provides valuable insights, it is not the exclusive method for analyzing brain activity induced by cognitive tasks. Specifically, conventional model-free ISC (response-ISC) relies on direct comparisons of brain response patterns between individuals[49]. The response-ISC exhibited a similar pattern to the weight-ISC ($r = 0.927$; Supplementary Fig. 12a, b), indicating relatively large values in the sensorimotor areas. In contrast, the response-ISC showed less consistency with the RSM-ISC ($r = 0.725$; Supplementary Fig. 12c), likely due to deviations in the fronto-parietal and higher-order visual cortices. These results suggest that subject-invariant cognitive structures can be revealed through model-based RSM-ISC analysis, distinct from conventional ISC analysis.

Within the model-based approach, alternative models incorporating latent visual and language features could be considered. All tasks, even auditory and motor tasks, contained visual information in the form of instructional text. Recent advances in ANNs allow the extraction of latent features from stimuli, enabling the decomposition of categorical tasks based on these latent variables[48]. Consequently, we extracted latent visual features using a visual transformer (ViT) and language features using GPT-NeoX from presented images and instruction texts, respectively, constructing additional encoding models (Fig. 5a). It is important to note that the goal of this analysis was not to identify the optimal model for cognitive tasks, and the two types of features selected here serve as examples of latent features. These encoding models significantly predicted vertices across the cortex for both intra-subject prediction (ViT; prediction accuracy = 0.139 ± 0.023; 96.2% of vertices were significant; GPT-NeoX; prediction accuracy = 0.148 ± 0.025; 97.2% of vertices were significant; sign permutation test, corrected $p < 0.05$) and cross-subject prediction (ViT; prediction accuracy = 0.048 ± 0.007; 93.4% of vertices were significant; GPT-NeoX; prediction accuracy = 0.050 ± 0.007; 94.6% of vertices were significant) (Supplementary Fig. 13). These findings suggest that both visual and language latent features can capture brain activity patterns associated with the diverse cognitive tasks used in the present study.

Finally, we investigated whether the brain organization of cognitive structures is influenced by the latent features employed. Similar to the task-type features, we observed larger RSM-ISC than weight-ISC values in nonsensory areas (bilateral SOG, MTG, PreCS, and SPL) (difference between RSM- and weight-ISC; ViT, 0.030 ± 0.015; GPT-NeoX, 0.143 ± 0.020) for both visual and language models (Fig. 5b, c, Supplementary Fig. 14). Additionally, we identified smaller RSM-ISC values in sensorimotor areas (bilateral OP, HG, CS) (difference between RSM- and weight-ISC; ViT, −0.065 ± 0.032; GPT-NeoX, −0.025 ± 0.035). The distribution of the ISC difference (i.e., RSM- vs. weight-ISC) was narrower than that of the task-type model (standard deviation; task-type model, 0.142; ViT model, 0.047; GPT-NeoX, 0.078; Fig. 5d). Meanwhile, the encoding model based on the language features (GPT-NeoX) yielded a distribution more on the positive side, with larger RSM-ISC values. These results suggest that, while the proposed methods demonstrate robustness, their patterns can vary depending on the properties of the selected features. Notably, a narrower distribution suggests that the distinctions between weight-ISC and RSM-ISC are less pronounced when using latent ANN features.

Discussion

We have successfully demonstrated the effectiveness of our proposed method, RSM-ISC, in quantitatively assessing individual variability in cognitive structures. In this context, "cognitive structure" refers to a collection of representational similarities among 25 cognitive tasks, indicating whether pairs of tasks exhibit similar multivoxel activation patterns. In contrast, weight-ISCs, which involve a direct comparison of multivoxel patterns for each task across subjects, lack information regarding multivoxel pattern similarity across tasks. Moreover, while weight-ISC is confined to the spatial arrangement of brain activity patterns, RSM-ISC captures individual differences in the representational space based on similarity

measures, presenting information abstracted from anatomical structures and activity patterns. The observed differences in cortical patterns between RSM-ISC and weight-ISC can be attributed to the impact of such constraints.

The key characteristic of RSM-ISC is that it handles information about the relationship between multiple tasks. As shown in Fig. 1a, language and visual tasks may be closely represented in a single brain, but their representational distances may be far apart for another's brain. Such relational information cannot be captured by the weight-ISC because this technique directly compares the weights of given tasks (averaged across vertices or extracted from a single vertex), without considering the similarity of these tasks in terms of spatial patterns. Even if some tasks have similar average weight values between two individuals, their spatial patterns are not necessarily similar (and their representational distance may be far apart). Further, the importance of relational information in measuring individual variability, particularly based on stimulus similarity judgments, has been suggested in behavioral research[52–54]. For all the above, our methodology could be useful in linking behavioral similarity data to brain representations.

The RSM-ISC approach stands apart from conventional ISC literature, which typically involves the direct comparison of temporal dynamics of brain activity between subjects during activities like movie viewing or story listening[16,17,21,49], yielding outcomes akin to weight-ISC. In the categorical task-type model, where cognitive tasks are treated as independent elements, model weights alone may not extract information beyond model-free brain activity. Although some studies have explored ISC based on spatial multivoxel patterns of brain activity[55,56] and the similarity of multivoxel patterns between different time points[57,58] or different events[35], our method differs by not directly comparing activity patterns of cognitive tasks but rather focusing on the relations between model weights.

It should be noted that RSM-ISC is not always favored over weight-ISC or response-ISC, as both methods shed light on different aspects of brain representation and brain activity. For example, a 2-D map of 25 different tasks can be obtained by performing a PCA on the original weight matrix (Supplementary Fig. 8), which cannot be obtained with the RSM. In addition, there are several studies that use response-ISC as an SNR[59,60], but such direct comparison of brain activities is not possible with RSM. Thus, we believe that RSM-ISC is superior to other methods for examining individual differences in brain representations across many cognitive functions (i.e., cognitive structures), but weight-ISC or response-ISC may be more appropriate depending on the aim of the analysis.

The inclusion of diverse tasks in our experimental design was crucial for implementing RSM-ISC. Without such tasks, it would be challenging to assess whether individuals' cognitive structures are similar or different, particularly concerning functions like language and auditory processing. Unlike our previous studies[27,28], where a small group performed 103 tasks over a 3-day MRI experiments, the current study, involving 59 subjects performing 25 tasks in a 30 min session, efficiently allowed us to capture cognitive structures across a larger subject pool. Despite its simple design, our encoding model effectively showed significant prediction (i.e., larger than chance level across subjects) over 90% of cortical vertices, indicating that the selected 25 tasks covered diverse activity patterns in the cerebral cortex. Nevertheless, we observed that subjects can be accurately identified with at least 14 tasks, indicating the potential for optimizing the task set to more efficiently estimate cognitive structures in a shorter timeframe.

One might argue that individual differences in brain activity patterns (and reduced cross-subject prediction accuracy) stem from insufficient functional alignment across subjects, and that the hyperalignment technique could reduce such individual variability[4,61–63]. A previous study employing semantic encoding models demonstrated that hyperalignment improved cross-subject prediction compared to anatomical alignment[62]. Furthermore, hyperalignment has been shown to increase the reliability of detecting subject-specific activity patterns[4,63] and to enhance the prediction of individual behavioral scores[61]. Although the present study conducted analyses exclusively based on anatomical alignment, incorporating hyperalignment may yield more accurate estimates of subject-specific brain activity patterns, thereby improving cross-subject prediction performance. It remains to be determined whether hyperalignment enhances both weight-ISC and RSM-ISC, or whether it accentuates the differences between them.

The searchlight analysis employing RSM-ISC revealed cortical patterns that contrast with findings from previous studies on individual variability and similarity[8,9,24,25]. Notably, in our study, RSM-ISC exhibited larger values in the higher-order areas (bilateral SOG, MTG, PreCS, and SPL), while showing smaller values in the low-level sensorimotor networks (bilateral OP, HG, and CS). Several studies have associated the fronto-parietal control network with general cognitive abilities, such as executive functions[64,65]. This network has been considered a "hub" connecting various cognitive functions and facilitating task switching[50,66,67], suggesting systematic connections to diverse cognitive tasks across individuals. Although the higher-order visual cortex may not traditionally be seen as a cognitive hub, a recent study suggests its involvement in the integration of multimodal information[68]. Particularly in the current study, where task instructions were presented in text, the integration of visual and linguistic information may play a crucial role in processing cognitive tasks.

Further insights into the distinct roles of these networks were gained through PCA. A representative vertex from the fronto-parietal network exhibited discrete task clusters, while another vertex from the higher-order visual network showed intertwined relations. These results underscore the heterogeneity in cognitive structures even within subject-invariant networks. Notably, in the higher visual network, tasks within the same cluster often exhibited considerable dissimilarity in representational similarity. In contrast, most tasks within the same cluster demonstrated a similar representation in the fronto-parietal network. This suggests that in the latter network, cognitive tasks may be represented in a compressed form based on higher-order functional units or clusters, transcending superficial differences in visual stimuli, presentation time, and textual information.

The exploration of additional encoding models revealed that the model-based approach extended beyond discrete task-type features to include other latent features. The use of latent features from intermediate ANN layers has been prevalent in studies investigating the correspondence between ANNs and the brain[48,69,70]. Given that latent features can be extracted from complex naturalistic stimuli like audio or movies, our approach holds potential for broader applicablity to various task-fMRI datasets. It could reveal individual differences not only in general cognitive structures but also in specific cognitive function structures, such as those related to object perception.

Additionally, the RSM-ISC may help explore the extent to which latent features contain information about cognitive structures. For example, ViT features produced a median value comparable to that of the task-type feature, as observed on the cortical map (Fig. 5b). It is possible that ViT and task-type features had common visual information, which led to the similar RSM- vs. weight-ISC values. Typically, tasks in the auditory and introspection domains do not contain visual images or sentences, and may have information related to the type of cognitive task in the form of "lack of visual stimuli." In contrast, GPT-NeoX features produced a larger RSM-ISC than weight-ISC across the cortex, and RSM-ISC and weight-ISC had an identical value around the CS (Fig. 5c). This may be because GPT-NeoX features contain linguistic information and rely less on lower order sensory information, increasing RSM-ISC values. Conversely, weight-ISC may have smaller values using GPT-NeoX features because it reflects sensory information.

The narrower distributions observed in both visual and language features might arise from the shared visual and language components across the 25 tasks. All cognitive tasks contain visual and verbal information (task instructions are provided in text), and each ViT and GPT-NeoX latent feature may partially contribute to all cognitive tasks. Therefore, the latent visual and language features could bridge multiple cognitive tasks through their shared components, even as the weight-ISC (without calculating RSM-ISC). Such a property of latent features may have made RSM-ISC less distinguishable from weight-ISC.

However, there are several limitations to the current study. First, while the 25 tasks adequately explained the activity of most cortical areas, this task set did not encompass certain crucial cognitive factors like odor perception or social communication. Components of cognitive structures related to such tasks may be absent from our analysis. Nevertheless, our method's advantage lies in its applicability regardless of task type and model, enabling the investigation of individual variability in a wide range of cognitive components once relevant task-fMRI data is available.

Second, without the subtraction of weight-ISC, the raw RSM-ISC itself may not effectively distinguish cognitive structures in different cortical regions. As demonstrated in the simulation analysis, a group of vertices with similar model weight patterns across subjects may spontaneously generate high RSM-ISC values. The raw RSM-ISC includes the weight-ISC component as a confounder, obstructing the accurate quantification of individual differences in cognitive structures in their original form. To enhance the robustness of our results, further methodological development is necessary to separate cognitive structures from other components.

Finally, there may be a more suitable metric to assess cognitive structures than RSM. RSM captures relational information based on the similarity of multivoxel patterns[26]. While widely used to test cognitive theories[31], this technique assumes that cognitive information is represented as spatial activity patterns akin to population coding, overlooking the potential existence of other information formats, such as connectivity profiles and temporal dynamics. For example, the concept of *model connectivity* in Meschke et al. is based on similarity relations of encoding model weights (model connectivity) but focused on similarity among vertices rather than similarity among features[71]. This method thus captures a complementary aspect of similarity relations ignored in the current study. Moreover, the low temporal resolution of fMRI data poses a limitation for examining temporal dynamics, and it is unclear whether the current methodology is applicable to other types of neuroimaging data with higher temporal resolution.

Conclusions

The present study introduces a methodology for assessing individual similarity and variability in abstract cognitive structures by incorporating RSA and ISC. The findings highlight the involvement of higher-order cortical regions in shaping common cognitive structures across individuals. This research offers a fresh perspective on the neural basis of individual differences, highlighting the necessity for future research utilizing the present methodology to elucidate the origins of the disparities observed in comparison to prior investigations.

Methods

Subjects

Fifty-nine subjects, aged 20–55 years (19 females, all with normal vision), denoted as ID01–ID59, participated in this study. Written informed consent was obtained from all subjects before their participation, and the study received approval from the ethics and safety committee of the National Institute of Information and Communications Technology in Osaka, Japan. All ethical regulations relevant to human research participants were followed.

Stimuli and procedures

We designed 25 naturalistic tasks that required no pre-experimental training (see Supplementary Note 5 for detailed task descriptions and Supplementary Table 2 and Supplementary Note 2 for behavioral results). These tasks, derived from our prior studies[27,28], were crafted to encompass a broad spectrum of cognitive domains (memory, language, introspection, auditory, motor, visual) within a 30 min experimental session. Each task comprised ten instances, with eight instances used in the training runs and two in the test run. Stimuli were presented on a projector screen inside the scanner (21.0 × 15.8° of visual angle at 30 Hz), and the root-mean-square of auditory stimuli was normalized. Subjects, equipped with MR-compatible ear tips. Presentation software (Neurobehavioral Systems, Albany, CA, USA) was used to control the stimulus presentation and the collection of behavioral data. To measure button responses, optic response pads with two buttons in each hand were used (HHSC-2 × 2, Current Designs, Philadelphia, PA, USA).

The experiment comprised ten runs, with half dedicated to task-based fMRI (task-fMRI) and the remaining half to resting-state fMRI (rest-fMRI). The rest-fMRI data was not analyzed in the current study. Each task-fMRI run included 50 trials (two trials for each of the 25 tasks), lasting 6–10 s per trial. Additionally, 10 s of scanning without a task was inserted at the beginning and end of each run; the former was excluded from the analysis. Both task-fMRI and rest-fMRI runs had a duration of 370 s. The task order was pseudorandomized, considering dependencies between certain tasks, such as the "MemoryLetter" and "MatchLetter" tasks, which were presented close to each other in time. The run order was counter-balanced across subjects. During task-fMRI runs, subjects received instructions on how to perform each task through instructional text presented as part of the stimuli (see Fig. 1b). Subjects underwent a brief training session on button responses.

MRI data acquisition

The experiment was conducted using a 3.0 T scanner (MAGNETOM Vida; Siemens, Erlangen, Germany) with a 64-channel head coil. We scanned 72 interleaved axial slices, 2 mm thick without a gap, parallel to the anterior and posterior commissure line, using a T2*-weighted gradient-echo multiband echo-planar imaging sequence [repetition time (TR) = 1000 ms; echo time (TE) = 30 ms; flip angle (FA) = 62°; field of view (FOV) = 192 × 192 mm^2; resolution = 2 × 2 mm^2; multiband factor = 6]. We obtained 370 volumes in each run, each following 10 dummy volumes. As an anatomical reference, high-resolution T1-weighted images of the whole brain were acquired from all subjects with a magnetization-prepared rapid acquisition gradient-echo sequence (TR = 2530 ms; TE = 3.26 ms; FA = 9°; FOV = 256 × 256 mm^2; voxel size = 1 × 1 × 1 mm^3).

Preprocessing

The preprocessing of both functional and anatomical MRI data was carried out using fMRIPrep 21.0.2[72]. A B0 fieldmap was derived from phase-drift maps, which were measured using two successive gradient-recalled echo acquisitions. The corresponding phase maps were unwrapped using prelude (FSL 6.0.5.1).

The T1-weighted image underwent a correction for intensity non-uniformity using ANTs 2.3.3 N4BiasFieldCorrection[73]. Following this, the image was skull-stripped using a Nipype implementation of the antsBrainExtraction.sh workflow. Brain tissue segmentation was conducted using fast (FSL 6.0.5.1)[74]. Brain surfaces were reconstructed using recon-all (FreeSurfer 6.0.1)[75]. Lastly, volume-based spatial normalization to the standard space (MNI152NLin6Asym) was achieved through nonlinear registration with antsRegistration (ANTs 2.3.3).

For functional scans, a reference volume and its skull-stripped version were initially produced using the custom methodology of fMRIPrep. Prior to spatiotemporal filtering, head-motion parameters, including six rotation and translation parameters, were estimated in relation to the reference scan using mcflirt (FSL 6.0.5.1)[76]. All functional scans underwent slice-time correction to the middle slice using 3dTshift from AFNI[77]. The reference scan was subsequently co-registered with the T1w reference using bbregister (FreeSurfer)[78]. Three global signals were extracted within the cerebrospinal fluid (CSF), white matter (WM), and whole-brain masks. The blood oxygenation level-dependent time-series was resampled into a standard space (MNI152NLin6Asym). All resampling was conducted using a single interpolation step by composing all the relevant transformations (i.e., head-motion transform matrices, susceptibility distortion correction, and co-registrations to anatomical and output spaces).

The resulting functional data underwent high-pass filtering at 0.01 Hz and low-pass filtering at 0.15 Hz. Confounding factors, including six head-motion parameters, global signals from the CSF, WM, and whole-brain masks, as well as the derivative of each factor, were eliminated using linear regression implemented in Scikit-learn. The functional data were then

standardized to have a zero mean and unit variance for each of the 18,715 cortical vertices in the fsaverage5 space, excluding non-cortical vertices.

Task-type features

The task-type features consisted of 25 one-hot vectors. Each time bin was assigned a value of 1 or 0, indicating whether one of the 25 tasks was performed during that period.

Latent visual features (ViT)

Latent visual features were extracted using the vision transformer model (ViT; https://huggingface.co/docs/transformers/model_doc/vit)[79]. For each time bin, the output from the sixth layer (out of twelve layers) was extracted as visual features when each stimulus image was used as input. The resulting series of features were further reduced to 100 dimensions using a PCA.

Latent language features (GPT-NeoX)

Latent language features were extracted using the Japanese version of the transformer-based large language model, GPT-NeoX https://huggingface.co/docs/transformers/model_doc/gpt_neox_japanese)[80]. When the instruction text of each stimulus was used as input, the output from the sixteenth layer (out of a total of thirty-two layers) was extracted as language features. These resultant series of features were then further reduced to 100 dimensions using PCA.

Vertex-wise encoding model fitting

In the encoding model, each vertex's cortical activity was modeled using a finite impulse response model. This model captured the slow hemodynamic response and its association with neural activity[38,81]. The feature matrix, denoted as $\mathbf{F_E}$ and of dimensions $[T \times 6\,N]$, was constructed by concatenating sets of $[T \times N]$ feature matrices, with six temporal delays ranging from 2 to 7 s (where T = number of samples; N = number of features). The cortical response denoted as $\mathbf{R_E}$ and of dimensions $[T \times V]$, was then modeled by multiplying the feature matrix $\mathbf{F_E}$ by the weight matrix $\mathbf{W_E}$ of dimensions $[6\,N \times V]$ (where V = number of vertices).

$$R_E = F_E W_E$$

The weight matrix $\mathbf{W_E}$ was obtained using L2-regularized linear regression with the training dataset, which consisted of 1110–1480 samples depending on the subjects. The optimal regularization parameter was determined using five-fold cross-validation, where the regularization parameters varied from 1 to 10^6 across seven different values.

The test dataset comprised 370 samples. The accuracy of the predictions was evaluated using Pearson's correlation coefficient between the predicted and actual test samples. Statistical significance (one-sided) was calculated using a sign permutation test ($p < 0.05$), and multiple comparisons were corrected using the false-discovery rate (FDR) correction method[82]. Prediction accuracy was computed in both intra-subject and cross-subject manners. In the intra-subject prediction, the predicted samples and test samples were from the same subject. In the cross-subject prediction, the predicted samples and test samples were from different subjects. Significant cortical vertices in the inter-subject prediction were used as an inclusive mask in subsequent analyses. For visualizing data on cortical maps, we utilized pycortex[83].

Whole cortex RSM

A whole-cortex RSM was obtained by calculating Pearson's correlation coefficient (r) between all pairs of task weight vectors. These vectors contained data on all vertices, corresponding to the rows of the weight matrix, and were averaged for the six temporal delays. The resulting $[25 \times 25]$ matrix shows how task pairs are similar or distinct ($r = 1$: perfectly similar; $r = -1$: perfectly distinct).

Subject identification analysis

We conducted a subject identification analysis to assess whether RSMs contain enough information to differentiate between subjects. The original training data was initially split into two samples (comprising the 1st and 2nd runs and the 3rd and 4th runs). RSMs were computed for both samples, and their upper triangular matrices were compared using Pearson's correlation coefficient. Specifically, correlation coefficients were calculated in both within-subject and cross-subject manners. A subject was deemed to be successfully identified if their within-subject correlation coefficient was larger than the cross-subject correlation coefficients between that subject and all other subjects.

We further repeated this analysis by incrementally increasing the number of tasks included in the RSMs from 3 to 24 (noting that we need at least three tasks to vectorize the upper triangular matrices). Target tasks were randomly selected from the original 25 tasks, and the mean identification accuracy across subjects was calculated. This process was repeated 100 times for each number of tasks.

ISC analysis

To quantitatively assess the extent to which different subjects exhibit similar brain activity or representations, we employed three distinct methods for computing ISC: (1). Weight-ISC: ISC was directly computed from the weight matrices obtained from the vertex-wise encoding models. Weight vectors were extracted from vertices within a 9 mm geodesic distance around each target vertex on the cortical surface (i.e., a searchlight sphere). The surface searchlight radius was determined based on previous research[4]. The resulting weight vectors, representing 25 task elements, were averaged across six temporal delays and within the target searchlight. Subsequently, ISC was computed at each target vertex by calculating Pearson's correlation coefficient between the mean weight vectors of all subject pairs (a total of 1711 pairs) and then averaging across subject pairs. (2) RSM-ISC: individuals' RSM was initially calculated by computing Pearson's correlation coefficient between all pairs of task weight vectors extracted from the weight matrix within the target searchlight sphere. These weight vectors were not averaged across searchlight vertices, and the number of elements corresponded to the number of vertices. ISC was then computed based on the vectorized upper triangular part of the RSMs in a manner similar to weight-ISC. To ensure the robustness of the method, an additional analysis was performed using Spearman's correlation coefficient as a similarity index. (3) Response-ISC: brain response data from all training runs were concatenated and averaged across vertices within the target searchlight sphere. ISC was computed based on the concatenated response data for each target searchlight. Note that, although response-ISC and weight ISC could be calculated solely based on the central vertex, we averaged within the searchlight to make a fair comparison with the searchlight-based RSM-ISC by using the same set of vertices.

ISC simulation

To investigate the relationship between weight-ISC and RSM-ISC, we conducted simulations of weight matrices. To ensure that the simulation better reflects the variability of real data, we first calculated the SD of the weight matrices both across tasks (σ_{task}) and subjects (σ_{sub}). We created a reference weight matrix with 46 vertices ([25,46] matrix) where the weight values adhered to a normal distribution with mean = 0 and SD = σ_{task}. The number of vertices was determined based on the average number of searchlight vertices across the cortex. Using this reference weight matrix (denoted as X_{ref}), we generated a dataset of 59 entries (matching the number of subjects in the current experiment) by varying the SNR value from 0 to 1 in increments of 0.05:

$$X_i = X_{ref} \cdot SNR + \varepsilon_i \cdot (1 - SNR)$$

Where ε_i represents a random noise matrix following a normal distribution with mean = 0 and SD = σ_{sub}, and X_i denotes the simulated data for the ith subject. We computed the weight-ISC and RSM-ISC using these X_i s for

each SNR value. The resulting simulated plot was then fitted with a quadratic polynomial function using a least-square fitting method.

Multidimensional scaling

To visualize the representational relationships among subjects, we employed MDS. We used the ISC value as a distance metric, also known as correlation distance. MDS can map different subjects onto a two-dimensional space based on their correlation distances, positioning subjects with high correlation coefficients closer together. However, one limitation of MDS is that maps from different sources (weight-ISC and RSM-ISC) cannot be directly compared. To address this issue, we adopted individual difference scaling (IDIOSCAL)[84]. IDIOSCAL accounts for scaling variations due to different sources by using a weighted distance, thereby enabling the mapping of both weight-ISC and RSM-ISC of the 59 subjects onto the same two-dimensional space. This analysis was conducted using the SMACOF package in R[85].

PCA

To explore the different cognitive structures on the cortical surface, we conducted a PCA based on the vectorized upper triangular part of the RSMs, which had ${}_{25}C_2 = 300$ dimensions. We only considered vertices that exhibited a significantly larger RSM-ISC than weight-ISC, with a significance level of $p < 0.05$ (determined by a sign permutation test with FDR correction). The vectorized RSMs were concatenated across all included vertices, and PCA was applied to the concatenated matrix. To visualize the cortical organization of the cognitive structures, we extracted and normalized the PCA scores from each vertex. The resulting cortical map indicated the relative contribution of each cortical vertex to the top three PCs. The cognitive structure of the 25 tasks was further visualized as a network at each vertex based on their searchlight RSM, with a threshold of $r = 0.2$.

Statistics and reproducibility

Statistical significance of encoding models and RSM- vs. weight-ISC contrasts ($n = 59$, one-sided, 370 test samples for each subject) was calculated using a sign permutation ($p < 0.05$), and multiple comparisons were corrected using the FDR correction method[82].

Reporting summary

Further information on research design is available in the Nature Portfolio Reporting Summary linked to this article.

Data availability

The preprocessed brain data and stimulus features used in the current study are available on Zenodo (https://zenodo.org/records/10581223)[86]. Source data underlying Figs. 2c, d, 3c, 4b, and 5d are provided in Supplementary Data 1. Other data are available from the corresponding author on reasonable request.

Code availability

The analysis code used in the current study is available on Zenodo (https://zenodo.org/records/10581223)[86].

Received: 17 May 2024; Accepted: 25 April 2025;
Published online: 08 May 2025

References

1. Dubois, J. & Adolphs, R. Building a science of individual differences from fMRI. *Trends Cogn. Sci.* **20**, 425–443 (2016).
2. Seghier, M. L. & Price, C. J. Interpreting and utilising intersubject variability in brain function. *Trends Cogn. Sci.* **22**, 517–530 (2018).
3. Michon, K. J., Khammash, D., Simmonite, M., Hamlin, A. M. & Polk, T. A. Person-specific and precision neuroimaging: current methods and future directions. *Neuroimage* **263**, 119589 (2022).
4. Feilong, M., Nastase, S. A., Guntupalli, J. S. & Haxby, J. V. Reliable individual differences in fine-grained cortical functional architecture. *Neuroimage* **183**, 375–386 (2018).
5. Wang, D. et al. Parcellating cortical functional networks in individuals. *Nat. Neurosci.* **18**, 1853–1860 (2015).
6. Gordon, E. M. et al. Precision functional mapping of individual human brains. *Neuron* **95**, 791–807 (2017).
7. Gratton, C. et al. Functional brain networks are dominated by stable group and individual factors, not cognitive or daily variation. *Neuron* **98**, 439–452 (2018).
8. Mueller, S. et al. Individual variability in functional connectivity architecture of the human brain. *Neuron* **77**, 586–595 (2013).
9. Vanderwal, T. et al. Individual differences in functional connectivity during naturalistic viewing conditions. *Neuroimage* **157**, 521–530 (2017).
10. Seitzman, B. A. et al. Trait-like variants in human functional brain networks. *Proc. Natl. Acad. Sci.***116**, 22851–22861 (2019).
11. Cutts, S. A., Faskowitz, J., Betzel, R. F. & Sporns, O. Uncovering individual differences in fine-scale dynamics of functional connectivity. *Cereb. Cortex* **33**, 2375–2394 (2022).
12. Cui, Z. et al. Individual variation in functional topography of association networks in youth. *Neuron* **106**, 340–353 (2020).
13. Stoecklein, S. et al. Variable functional connectivity architecture of the preterm human brain: impact of developmental cortical expansion and maturation. *Proc. Natl. Acad. Sci.***117**, 1201–1206 (2020).
14. Margulies, D. S. et al. Situating the default-mode network along a principal gradient of macroscale cortical organization. *Proc. Natl. Acad. Sci.***113**, 12574–12579 (2016).
15. Keller, A. S. et al. Hierarchical functional system development supports executive function. *Trends Cogn. Sci.* **27**, 160–174 (2023).
16. Hasson, U., Nir, Y., Levy, I., Fuhrmann, G. & Malach, R. Intersubject synchronization of cortical activity during natural vision. *Science* **303**, 1634–1640 (2004).
17. Hasson, U., Furman, O., Clark, D., Dudai, Y. & Davachi, L. Enhanced intersubject correlations during movie viewing correlate with successful episodic encoding. *Neuron* **57**, 452–462 (2008).
18. Chang, L. J. et al. Endogenous variation in ventromedial prefrontal cortex state dynamics during naturalistic viewing reflects affective experience. *Sci. Adv.* **7**, eabf7129 (2021).
19. Wilson, S. M., Molnar-Szakacs, I. & Iacoboni, M. Beyond superior temporal cortex: intersubject correlations in narrative speech comprehension. *Cereb. Cortex* **18**, 230–242 (2008).
20. Abrams, D. A. et al. Inter-subject synchronization of brain responses during natural music listening. *Eur. J. Neurosci.* **37**, 1458–1469 (2013).
21. Simony, E. et al. Dynamic reconfiguration of the default mode network during narrative comprehension. *Nat. Commun.* **7**, 12141 (2016).
22. Silbert, L. J., Honey, C. J., Simony, E., Poeppel, D. & Hasson, U. Coupled neural systems underlie the production and comprehension of naturalistic narrative speech. *Proc. Natl. Acad. Sci.***111**, E4687–E4696 (2014).
23. Setti, F. et al. A modality-independent proto-organization of human multisensory areas. *Nat. Hum. Behav.* **7**, 397–410 (2023).
24. Ren, Y., Nguyen, V. T., Guo, L. & Guo, C. C. Inter-subject functional correlation reveal a hierarchical organization of extrinsic and intrinsic systems in the brain. *Sci. Rep.* **7**, 10876 (2017).
25. Kauppi, J.-P., Pajula, J., Niemi, J., Hari, R. & Tohka, J. Functional brain segmentation using inter-subject correlation in fMRI. *Hum. Brain Mapp.* **38**, 2643–2665 (2017).
26. Kriegeskorte, N. & Kievit, R. A. Representational geometry: integrating cognition, computation, and the brain. *Trends Cogn. Sci.* **17**, 401–412 (2013).
27. Nakai, T. & Nishimoto, S. Quantitative models reveal the organization of diverse cognitive functions in the brain. *Nat. Commun.* **11**, 1142 (2020).

28. Nakai, T. & Nishimoto, S. Representations and decodability of diverse cognitive functions are preserved across the human cortex, cerebellum, and subcortex. *Commun. Biol.* **5**, 1245 (2022).
29. Kriegeskorte, N., Goebel, R. & Bandettini, P. Information-based functional brain mapping. *Proc. Natl. Acad. Sci.***103**, 3863–3868 (2006).
30. Devereux, B. J., Clarke, A., Marouchos, A. & Tyler, L. K. Representational similarity analysis reveals commonalities and differences in the semantic processing of words and objects. *J. Neurosci.* **33**, 18906–18916 (2013).
31. Peelen, M. V. & Downing, P. E. Testing cognitive theories with multivariate pattern analysis of neuroimaging data. *Nat. Hum. Behav.* **7**, 1430–1440 (2023).
32. Charest, I., Kievit, R. A., Schmitz, T. W., Deca, D. & Kriegeskorte, N. Unique semantic space in the brain of each beholder predicts perceived similarity. *Proc. Natl. Acad. Sci.***111**, 14565–14570 (2014).
33. Brooks, J. A., Chikazoe, J., Sadato, N. & Freeman, J. B. The neural representation of facial-emotion categories reflects conceptual structure. *Proc. Natl. Acad. Sci.***116**, 15861–15870 (2019).
34. Finn, E. S. et al. Idiosynchrony: from shared responses to individual differences during naturalistic neuroimaging. *Neuroimage* **215**, 116828 (2020).
35. de Bruin, D., van Baar, J. M., Rodríguez, P. L. & FeldmanHall, O. Shared neural representations and temporal segmentation of political content predict ideological similarity. *Sci. Adv.* **9**, eabq5920 (2023).
36. Naselaris, T., Kay, K. N., Nishimoto, S. & Gallant, J. L. Encoding and decoding in fMRI. *Neuroimage* **56**, 400–410 (2011).
37. Kay, K. N., Naselaris, T., Prenger, R. J. & Gallant, J. L. Identifying natural images from human brain activity. *Nature* **452**, 352–355 (2008).
38. Nishimoto, S. et al. Reconstructing visual experiences from brain activity evoked by natural movies. *Curr. Biol.* **21**, 1641–1646 (2011).
39. Çukur, T., Nishimoto, S., Huth, A. G. & Gallant, J. L. Attention during natural vision warps semantic representation across the human brain. *Nat. Neurosci.* **16**, 763–770 (2013).
40. Norman-Haignere, S., Kanwisher, N. G. & McDermott, J. H. Distinct cortical pathways for music and speech revealed by hypothesis-free voxel decomposition. *Neuron* **88**, 1281–1296 (2015).
41. Nakai, T., Koide-Majima, N. & Nishimoto, S. Correspondence of categorical and feature-based representations of music in the human brain. *Brain Behav.* **11**, e01936 (2021).
42. Horikawa, T., Cowen, A. S., Keltner, D. & Kamitani, Y. The neural representation of visually evoked emotion Is high-dimensional, categorical, and distributed across transmodal brain regions. *iScience* **23**, 101060 (2020).
43. Koide-Majima, N., Nakai, T. & Nishimoto, S. Distinct dimensions of emotion in the human brain and their representation on the cortical surface. *Neuroimage* **222**, 117258 (2020).
44. Huth, A. G., de Heer, W. A., Griffiths, T. L., Theunissen, F. E. & Gallant, J. L. Natural speech reveals the semantic maps that tile human cerebral cortex. *Nature* **532**, 453–458 (2016).
45. Nishida, S. & Nishimoto, S. Decoding naturalistic experiences from human brain activity via distributed representations of words. *Neuroimage* **180**, 232–242 (2018).
46. Nakai, T., Yamaguchi, H. Q. & Nishimoto, S. Convergence of modality invariance and attention selectivity in the cortical semantic circuit. *Cereb. Cortex* **31**, 4825–4839 (2021).
47. Nakai, T. & Nishimoto, S. Quantitative modelling demonstrates format-invariant representations of mathematical problems in the brain. *Eur. J. Neurosci*. **57**, 1003–1017 (2023).
48. Nakai, T. & Nishimoto, S. Artificial neural network modelling of the neural population code underlying mathematical operations. *Neuroimage* **270**, 119980 (2023).
49. Nastase, S. A., Gazzola, V., Hasson, U. & Keysers, C. Measuring shared responses across subjects using intersubject correlation. *Soc. Cogn. Affect. Neurosci.* **14**, 667–685 (2019).
50. Ito, T. & Murray, J. D. Multitask representations in the human cortex transform along a sensory-to-motor hierarchy. *Nat. Neurosci*. 26, 306–315 (2022).
51. Schaefer, A. et al. Local-global parcellation of the human cerebral cortex from intrinsic functional connectivity MRI. *Cereb. Cortex* **28**, 3095–3114 (2018).
52. Roads, B. D. & Love, B. C. Modeling similarity and psychological space.*Annu. Rev. Psychol.* **75**, 215–240 (2024).
53. Shepard, R. & Chipman, S. Second-order isomorphism of internal representations: shapes of states. *Cogn. Psychol.* **1**, 1–17 (1970).
54. Tsuchiya, N. & Saigo, H. A relational approach to consciousness: categories of level and contents of consciousness. *Neurosci. Conscious.* **2021**, niab034 (2021).
55. Chen, J. et al. Shared memories reveal shared structure in neural activity across individuals. *Nat. Neurosci.* **20**, 115–125 (2017).
56. Sheng, J. et al. Intersubject similarity in neural representations underlies shared episodic memory content. *Proc. Natl. Acad. Sci.***120**, e2308951120 (2023).
57. Guntupalli, J. S. et al. A model of representational spaces in human cortex. *Cereb. Cortex* **26**, 2919–2934 (2016).
58. Guntupalli, J. S., Feilong, M. & Haxby, J. V. A computational model of shared fine-scale structure in the human connectome. *PLoS Comput. Biol.* **14**, e1006120 (2018).
59. Gu, Z., Jamison, K., Sabuncu, M. & Kuceyeski, A. Personalized visual encoding model construction with small data. *Commun. Biol.* **5**, 1382 (2022).
60. Kumar, S. et al. Shared functional specialization in transformer-based language models and the human brain. *Nat. Commun.* **15**, 5523 (2024).
61. Feilong, M., Guntupalli, J. S. & Haxby, J. V. The neural basis of intelligence in fine-grained cortical topographies. *Elife* **10**, e64058 (2021).
62. Van Uden, C. E. et al. Modeling semantic encoding in a common neural representational space. *Front. Neurosci.* **12**, 437 (2018).
63. Jiahui, G. et al. Predicting individual face-selective topography using naturalistic stimuli. *Neuroimage* **216**, 116458 (2020).
64. Niendam, T. A. et al. Meta-analytic evidence for a superordinate cognitive control network subserving diverse executive functions. *Cogn. Affect. Behav. Neurosci.* **12**, 241–268 (2012).
65. Friedman, N. P. & Robbins, T. W. The role of prefrontal cortex in cognitive control and executive function. *Neuropsychopharmacology* **47**, 72–89 (2022).
66. Cole, M. W. et al. Multi-task connectivity reveals flexible hubs for adaptive task control. *Nat. Neurosci.* **16**, 1348–1355 (2013).
67. Power, J. D., Schlaggar, B. L., Lessov-Schlaggar, C. N. & Petersen, S. E. Evidence for hubs in human functional brain networks. *Neuron* **79**, 798–813 (2013).
68. Popham, S. F. et al. Visual and linguistic semantic representations are aligned at the border of human visual cortex. *Nat. Neurosci.* **24**, 1628–1636 (2021).
69. Horikawa, T. & Kamitani, Y. Generic decoding of seen and imagined objects using hierarchical visual features. *Nat. Commun.* **8**, 15037 (2017).
70. Schrimpf, M. et al. The neural architecture of language: Integrative modeling converges on predictive processing. *Proc. Natl. Acad. Sci.* **118**, e2105646118 (2021).
71. Meschke, E. X., Visconti di Oleggio Castello, M., Dupré la Tour, T. & Gallant, J. L. Model connectivity: leveraging the power of encoding models to overcome the limitations of functional connectivity. *biorxiv.org* (2023).
72. Esteban, O. et al. fMRIPrep: a robust preprocessing pipeline for functional MRI. *Nat. Methods* **16**, 111–116 (2019).
73. Avants, B. B. et al. A reproducible evaluation of ANTs similarity metric performance in brain image registration. *Neuroimage* **54**, 2033–2044 (2011).

74. Zhang, Y., Brady, M. & Smith, S. Segmentation of brain MR images through a hidden Markov random field model and the expectation-maximization algorithm. *IEEE Trans. Med. Imaging* **20**, 45–57 (2001).
75. Dale, A.M., Fischl, B. & Sereno, M.I. Cortical surface-based analysis. Segmentation and surface reconstruction. *Neuroimage* **9**, 179–194 (1999).
76. Jenkinson, M., Bannister, P., Brady, M. & Smith, S. Improved optimization for the robust and accurate linear registration and motion correction of brain images. *Neuroimage* **17**, 825–841 (2002).
77. Cox, R. W. & Hyde, J. S. Software tools for analysis and visualization of fMRI data. *NMR Biomed.* **10**, 171–178 (1997).
78. Greve, D. N. & Fischl, B. Accurate and robust brain image alignment using boundary-based registration. *Neuroimage* **48**, 63–72 (2009).
79. Dosovitskiy, A. et al. An image is worth 16x16 words: Transformers for image recognition at scale. *Int. Conf. Learn. Represent.* (2021).
80. Black, S. et al. GPT-NeoX-20B: An open-source autoregressive language model. *Proc. BigScience Episode #5 – Workshop on Challenges & Perspectives in Creating Large Language Models*, 95–136 (2022).
81. Kay, K. N., David, S. V., Prenger, R. J., Hansen, K. A. & Gallant, J. L. Modeling low-frequency fluctuation and hemodynamic response timecourse in event-related fMRI. *Hum. Brain Mapp.* **29**, 142–156 (2008).
82. Benjamini, Y. & Hochberg, Y. Controlling the false discovery rate: A practical and powerful approach to multiple testing. *J. R. Stat. Soc.* **57**, 289–300 (1995).
83. Gao, J. S., Huth, A. G., Lescroart, M. D. & Gallant, J. L. Pycortex: an interactive surface visualizer for fMRI. *Front. Neuroinform.* **9**, 23 (2015).
84. Carroll, J. D. & Chang, J.-J. Analysis of individual differences in multidimensional scaling via an n-way generalization of "Eckart-Young" decomposition. *Psychometrika* **35**, 283–319 (1970).
85. de Leeuw, J. & Mair, P. Multidimensional scaling using majorization: SMACOF in R. *J. Stat. Softw.* **31**, 1–30 (2009).
86. Nakai, T. Kubo, R., & Nishimoto, S. Data and code: cortical representational geometry of diverse tasks reveals subject-specific and subject-invariant cognitive structures [Data set]. Zenodo. https://doi.org/10.5281/zenodo.10581223 (2025).

Acknowledgements

We thank MEXT/JSPS KAKENHI (grant numbers JP24H02172 and JP24H01559 for T.N., JP18H05522 and JP24H00619 for S.N.), JST ERATO JPMJER1801, AIP JPMJCR24U2 (for S.N.), JST FOREST Program (JPMJFR231V for T.N.), and H2020 Marie Skłodowska-Curie actions (grant number 101023033 for T.N.) for partial financial support of this study. The funders had no role in the study design, data collection and analysis, decision to publish, or preparation of the manuscript.

Author contributions

T.N.: Conceptualization, methodology, formal analysis, visualization, and writing—original draft preparation. R.K.: Data collection, writing—review and editing. S.N.: Supervision, writing—review and editing, and funding acquisition.

Competing interests

The authors declare no competing interests.

Additional information

Supplementary information The online version contains supplementary material available at https://doi.org/10.1038/s42003-025-08134-4.

Correspondence and requests for materials should be addressed to Tomoya Nakai.

Peer review information *Communications Biology* thanks the anonymous reviewers for their contribution to the peer review of this work. Primary handling editors: J.V. A peer review file is available.